ORIGINAL RESEARCH

Notch-Regulated c-Kit–Positive Liver Sinusoidal Endothelial Cells Contribute to Liver Zonation and Regeneration

Juan-Li Duan,[1,*] Zi-Yi Zhou,[2,*] Bai Ruan,[1,3,4,*] Zhi-Qiang Fang,[1] Jian Ding,[1] Jing-Jing Liu,[1] Ping Song,[1] Hao Xu,[1] Chen Xu,[1] Zhen-Sheng Yue,[1,2] Hua Han,[3] Guo-Rui Dou,[2] and Lin Wang[1,3]

[1]Department of Hepatobiliary Surgery, [2]Department of Ophthalmology, Xi-Jing Hospital, [3]State Key Laboratory of Cancer Biology, Department of Biochemistry and Molecular Biology, [4]Center of Clinical Aerospace Medicine, Department of Aviation Medicine, Fourth Military Medical University, Xi'an, China
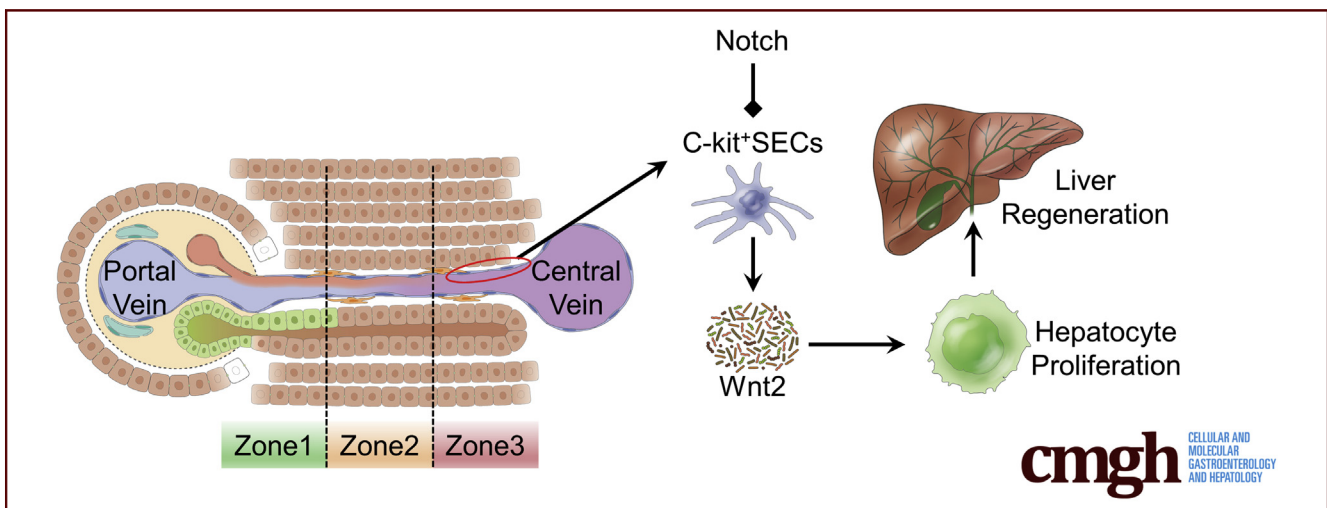
SUMMARY

c-Kit–positive liver sinusoidal endothelial cells promote hepatocyte proliferation and attenuate toxin-induced liver injuries. Notch mutation reshapes c-kit[+] sinusoidal endothelial cell spatial distribution, affecting liver zonation. Endothelial Notch activation impedes liver regeneration by abrogating c-kit[+] sinusoidal endothelial cell–derived wingless-type MMTV integration site family, member2 angiocrine.

BACKGROUND & AIMS: Liver sinusoidal endothelial cells (SECs) promote the proliferation of hepatocytes during liver regeneration. However, the specific subset of SECs and its mechanisms during the process remain unclear. In this study, we investigated the potential role of c-kit[+] SECs, a newly identified subset of SECs in liver regeneration.

METHODS: Partial hepatectomy mice models were established to induce liver regeneration. Hepatic c-kit expression was detected by quantitative reverse-transcription polymerase chain reaction, immunofluorescent staining, and fluorescence-activated cell sorting. VE-cadherin-cyclization recombinase-estrogen receptor (Cdh5-Cre-ERT) Notch intracellular domain and Cdh5-Cre recombination signal binding protein Jκ[floxp] mice were

introduced to mutate Notch signaling. c-Kit[+] SECs were isolated by magnetic beads. Single-cell RNA sequencing was performed on isolated SECs. Liver injuries were induced by CCl[4] or quantitative polymerase chain reaction injection.

RESULTS: Hepatic c-kit is expressed predominantly in SECs. Liver resident SECs contribute to the increase of c-kit during partial hepatectomy–induced liver regeneration. Isolated c-kit[+] SECs promote hepatocyte proliferation in vivo and in vitro by facilitating angiocrine. The distribution of c-kit shows distinct spatial differences that are highly coincident with the liver zonation marker wingless-type MMTV integration site family, member2 (Wnt2). Notch mutation reshapes the c-kit distribution and liver zonation, resulting in altered hepatocyte proliferation. c-Kit[+] SECs were shown to regulate hepatocyte regeneration through angiocrine in a Wnt2-dependent manner. Activation of the Notch signaling pathway weakens liver regeneration by inhibiting positive regulatory effects of c-kit[+] SECs on hepatocytes. Furthermore, c-kit[+] SEC infusion attenuates toxin-induced liver injuries in mice.

CONCLUSIONS: Our results suggest that c-kit[+] SECs contributes to liver zonation and regeneration through Wnt2 and is regulated by Notch signaling, providing opportunities for novel therapeutic approaches to liver injury in the future. Transcript profiling: GEO (accession number: GSE134037). *(Cell Mol Gastroenterol Hepatol 2022;13:1741–1756;* https://doi.org/10.1016/j.jcmgh.2022.01.019)

After injury, the liver has a strong ability to regenerate by stimulating the proliferation and hypertrophy of the remaining hepatocytes, completely restoring the volume and functions of the damaged liver.[1] The process of liver regeneration involves complex signaling pathways and a variety of cells.[2,3] Among them, liver sinusoidal endothelial cells (SECs) have been recognized to play pivotal roles in liver regeneration and adaptation to pathologic conditions.[4] SECs form a discontinuous fenestrated endothelial cell layer called sinusoidal vasculature, which enables free exchanges of fluid, ions, nutrients, small and large solutes, as well as metabolites with parenchymal liver cells (hepatocytes) and nonparenchymal cells (NPCs), such as hepatic stellate cells. Emerging evidence has shown that SECs show unique morphologic features and are functionally highly specialized.

Along the liver sinusoids, SECs are specialized according to liver zonation and categorized into pericentral, midlobular, and periportal subtypes. During liver regeneration, it is speculated that SECs from different zonations display diverse functions.[5–7] The intense, pericentral SECs adjacent to the central vein are the main source of the Wnt ligands Wnt2 and Wnt9, which play an essential role in hepatocyte proliferation.[8] In contrast, adjacent to the portal vein, CD157+ SECs undergo proliferative expansion after acute liver damage[9] and begin to proliferate and differentiate, which further reconstructs specific hepatic sinusoids. Notably, during this regenerative process, hepatic sinusoids not only provide the oxygen and nutrients to support the metabolic requirement of the liver, but also structure a fertile microenvironment-like niche, where SEC-derived angiocrine signals, such as Wnt2, hepatocyte growth factor (HGF), vascular endothelia growth factor receptor (VEGFR)1, atypical chemokine receptor 3 (CXCR7), Anpt2, and Gata4 contribute to the proliferation and differentiation of hepatocytes, as well as to liver function in both health and disease.[10–14]

c-Kit, also known as CD117, is a type III receptor tyrosine kinase[15] and a stem cell marker, whose significant role in c-kit+ cells across different organs has been widely discussed.[16] In the liver, hepatic resident stem cells and bone marrow–derived stem cells, both of which express c-kit, can differentiate into various cells according to specific injuries.[15] Furthermore, c-kit can be detected in several normal cells, including oval cells, bile epithelial cells, and part of hepatocytes.[17] C-kit+ cells play a key role in biliary disease–associated fibrogenesis.[15,18] The depletion of c-kit+ mast cells delay liver steatosis and fibrosis processes.[19] Moreover, the stem cell growth factor (SCF), which is a ligand of c-kit, was reported at increased levels during partial hepatectomy (PHx)-induced liver regeneration.[20,21] However, the complex role of c-kit+ cells remains largely unaddressed in studies, especially regarding c-kit+ SECs in liver regeneration.

In this study, we found that c-kit is expressed predominantly in SECs in the liver. PHx-induced regeneration repopulates liver resident c-kit+ cells, which enhances hepatocyte proliferation more efficiently via angiocrine pathways. Moreover, according to paired-cell sequencing, c-kit and Wnt2 show the same zonation-like spatial expression in the sinusoidal area, and they are both negatively regulated by endothelial Notch signaling. Impaired liver regeneration by Notch activation was rescued successfully by c-kit+ SEC infusion or exogenous Wnt2 overexpression. Finally, the implantation of c-kit+ SECs attenuates toxin-induced liver injuries. These findings indicate the potential therapeutic role of c-kit+ SECs in the treatment of liver injuries.

Results

Hepatic c-Kit Is Expressed Predominantly in SECs

Liver c-kit+ cells have been detected in multiple cell types, including some hepatocytes, Biliary epithelial cells, oval cells, and circulating progenitor cells during liver regeneration. Herein, we identify whether hepatic SECs likewise express c-kit. Single-cell RNA sequencing (RNA-seq) of the whole liver showed that SECs can be divided into 3 clusters, namely the portal vein (PV) SECs (zone 1), midlobular SECs (zones 2 and 3), and central vein (CV) SECs (Figure 1A). Interestingly, the c-kit cluster largely overlaps with liver endothelia, and most of the clusters are distributed in the areas of midlobular and central venous SECs (Figure 1B). To confirm these data, fluorescence-activated cell sorting (FACS) was used to analyze the total liver cells in terms of endothelial cell markers and c-kit. In CD146, CD31, and VEGFR2-positive liver endothelial cells, the proportions of c-kit+ cells were 71%, 78.9%, and 77.4%, respectively (Figure 1C), suggesting that c-kit is highly expressed in liver endothelial cells. We isolated the c-kit+ liver NPCs and performed scanning electronic microscopy and a lipid endocytosis assay.

SEC-specific fenestrae (Figure 1D) and endocytosis of 1,1-dioctadecyl-3,3,3,3-tetramethylindocarbocyanine perchlorate Acetylated low-density lipoprotein (Figure 1E) were observed in c-kit+ NPCs, indicating that these c-kit+ NPCs showed SEC-specific features. Immunofluorescent staining showed that c-kit colocalizes with SEC marker Lyve-1

Figure 1. Hepatic c-kit is expressed predominantly in SECs. (*A*) Total liver cells were analyzed by single-cell RNA-seq. (*B*) The distribution of liver endothelial cells is presented in the lower part, and the c-kit$^+$ cluster is shown. (*C*) FACS sorting and labeling of CD146$^+$, CD31$^+$, or VEGFR2$^+$ liver endothelial cells labeled with c-kit. (*D*) c-Kit$^+$ liver NPCs were sorted and analyzed by scanning electron microscopy. *Right*: Magnified view of the *left* image. (*E*) c-Kit$^+$ liver NPCs isolated and stained with Dil-Ac-LDL (red) and Hoechst (blue) in vitro. *Scale bar*: 50 μm. (*F*) Immunofluorescent staining of c-kit (red) and Lyve-1 (green) in normal liver. *Scale bar*: 50 μm. (*G*) mRNA expression of c-kit determined in c-kit$^+$ BM cells, hepatocytes (HCs), hepatic stellate cells (HSCs), Kupffer cells, and SECs by qRT-PCR (n = 3 per group). (*H*) c-Kit$^+$ proportion in CD146$^+$ SECs quantified by FACS. (*I*) Expression of VEGFR2, CD146, CD31, and CD45 measured in c-kit$^+$ SECs by FACS. *Bars* show means ± SD. ***P < .001. SSC, side scatter.

(Figure 1*F*). We further detected the messenger RNA (mRNA) levels of c-kit in hepatocytes, Kupffer cells, hepatic stellate cells, and SECs after isolation, and found that the c-kit expression in SECs was remarkably higher than in other cells (Figure 1*G*). These findings confirmed that the hepatic c-kit originated mainly from SECs. Furthermore, we tested
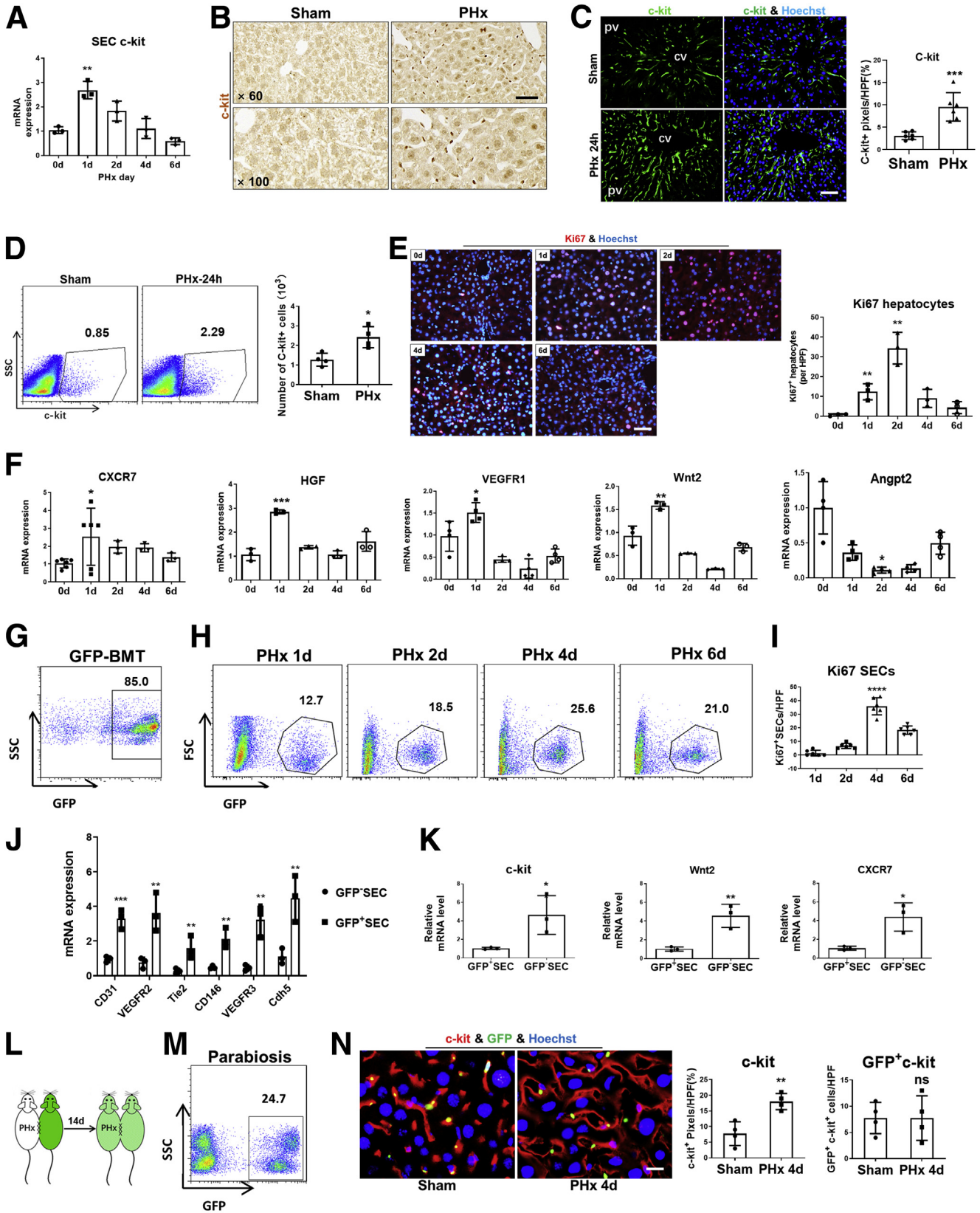
VEGFR3, CD146, CD31, and CD45 in c-kit$^+$ SECs. The positive proportions were 77%, 76.1%, 67.7%, and 95.7%, respectively (Figure 1I). These findings indicate that SECs are the principal source of hepatic c-kit expression. Next, we sorted SECs by CD146 magnetic beads and quantified their c-kit levels. A total of 69.4% of SECs were shown to be c-kit positive (Figure 1H).

Hepatic c-Kit Increases During Liver Regeneration

The expression of SEC c-kit then was investigated in PHx models. We detected the mRNA expression of c-kit in isolated SECs at different time points after PHx and found that c-kit reached the peak at day 1 (Figure 2A). In situ hybridization and immunofluorescent staining also showed that the expression of c-kit was significantly higher at 24 hours compared with the sham group after PHx (Figure 2B and C). Flow cytometry further confirmed that hepatic c-kit$^+$ cells increased on PHx day 1 (Figure 2D). The proliferation of hepatocytes peaked at 36–48 hours after PHx, which was confirmed in our study by anti-Ki67 staining (Figure 2E). The initiation of liver regeneration or hepatocyte proliferation occurred roughly around day 1 after PHx. The possibility that c-kit$^+$ SECs might initiate PHx-induced liver regeneration must be addressed in detail. To this end, we measured several known SEC-derived angiocrine factors, including CXCR7, HGF, VEGFR1, Wnt2, and Angpt2, at different time points during liver regeneration, and found that CXCR7, HGF, VEGFR1, and Wnt2 expression all were up-regulated at its initiation (Figure 2F). In parallel, Angpt2, which negatively control hepatocyte regeneration, showed significantly lower expression levels after PHx (Figure 2F). Therefore, we speculate that c-kit$^+$ SECs are required at the initiation of liver regeneration.

Liver Resident SECs Contribute to c-Kit Increase After PHx

To investigate whether bone marrow–derived c-kit$^+$ cells are involved in liver regeneration after PHx, green fluorescent protein (GFP) bone marrow transplant (BMT) chimeric mice models were established. Two months after transplantation,

the chimerism of BMT was investigated by FACS, showing that 85% of the recipients' bone marrow cells were GFP positive (Figure 2G). PHx was performed on GFP-BMT chimeric mice, and SECs were isolated by magnetic beads, while GFP$^+$ cells were obtained by using flow cytometry sorting. After PHx, the maximum proportion of GFP$^+$ SECs (25.6%) was observed on day 4 (Figure 2H), which is in sync with the peak of SEC proliferation (Figure 2I). Next, we compared the mRNA expression of endothelial markers and angiocrine factors between liver resident SECs and BM-derived SECs. The results showed that the expression of CD31, VEGFR2, TEK receptor tyrosine kinase (Tie 2), CD146, VEGFR3, Cdh5, Wnt2, and CXCR7 were significantly higher in GFP$^-$ SECs (Figure 2J and K). Importantly, c-kit was expressed predominantly in GFP$^-$ SECs (Figure 2K). To further confirm that hepatic c-kit expression originates from residential SECs, we established GFP-parabiosis models, as shown in Figure 2L. Fourteen days after the surgery, 24.7% of circulating cells were confirmed to be GFP positive (Figure 2M). Immunofluorescent staining showed significantly higher expression levels of hepatic c-kit after PHx, however, the GFP$^+$ c-kit levels indicated no difference between the 2 groups (Figure 2N), implying that circulating GFP$^+$ c-kit did not contribute to the increasing expression of hepatic c-kit. These findings indicate that liver resident SECs are the major source of higher hepatic c-kit levels after PHx.

c-Kit$^+$ SECs Promote Hepatocyte Proliferation In Vivo and In Vitro

According to the earlier-described findings, c-kit is related closely to hepatocyte regeneration. Thus, we generated endothelial cell–specific c-kit knockout mice (Cdh5-Cre Kit^{floxp}) to test this hypothesis. Unexpectedly, the depletion of endothelial c-kit did not affect hepatocyte proliferation and relative liver weight. Immunohistochemistry staining by Ki67 showed no difference between the Kit knockout and control group before or after PHx (Figure 3A). Isolated c-kit$^+$ and c-kit$^-$ SECs were harvested by magnetic beads and co-cultured with primary hepatocytes for 24 or 48 hours in vitro. Intriguingly, the amount of proliferating hepatocytes stained by Ki67 increased dramatically in the c-kit$^+$ SEC-treated group at different time points (Figure 3B).

Figure 2. (*See previous page*). **Liver resident c-kit increases during PHx-induced liver regeneration.** (*A*) Expression of c-kit in isolated SECs on different days after PHx determination by qRT-PCR (n = 3 per group). (*B* and *C*) Liver samples were collected from the sham and PHx group (24 hours after PHx). The expression levels of c-kit were analyzed by (*B*) ISH and (*C*) immunofluorescent staining (green) (n = 6 per group). *Scale bars*: 100 μm. (*D*) Hepatic c-kit$^+$ cells observed by FACS and quantified in the sham and the PHx group (n = 4 per group). (*E*) Liver samples of wild-type mice collected on days 0, 1, 2, 4, and 6 after PHx, co-stained with Ki67 (red) and Hoechst (blue), and quantified by counting Ki67$^+$ nuclei (pink). *Scale bar*: 50 μm (n = 3 per group). (*F*) Expression of CXCR7, HGF, VEGFR1, Wnt2, and Angpt2 on days 0, 1, 2, 4, and 6 after PHx determination by qRT-PCR (n = 3–6 per group). (*G*) GFP$^+$ BM cells transplanted to irradiated recipient mice and GFP$^+$ cells in peripheral blood of the recipients analyzed by FACS 2 months later. (*H*) GFP-BMT mice then were subjected to PHx, and GFP$^+$ SECs were isolated and quantified on days 1, 2, 4, and 6 after PHx by FACS. (*I*) Proliferation of SECs quantified on days 1, 2, 4, and 6 after PHx (n = 6 per group). (*J* and *K*) Expression of CD31, VEGFR2, TEK receptor tyrosine kinase, CD146, VEGFR3, Cdh5, c-kit, Wnt2, and CXCR7 compared between GFP$^+$ and GFP$^-$ SEC group by qRT-PCR on PHx day 4 (n = 3 per group). (*L*) Normal and GFP transgenic mouse cojoined by parabiosis surgery. (*M*) GFP$^+$ cells in PB of the normal mice were tested by FACS 14 days after parabiosis. (*N*) The untreated healthy mouse of the twin mice was subjected to PHx on day 14. Liver samples collected from the GFP-parabiosis models were stained with c-kit and Hoechst. The c-kit$^+$ (red) and c-kit$^+$GFP$^+$ (yellow) stain were statistically quantified between the sham and PHx group (n = 4 per group). *Scale bar*: 25 μm. *Bars* show means ± SD. *P < .05, **P < .01, ***P < .001, and ****P < .0001. HPF, high-power field; SSC, side scatter.
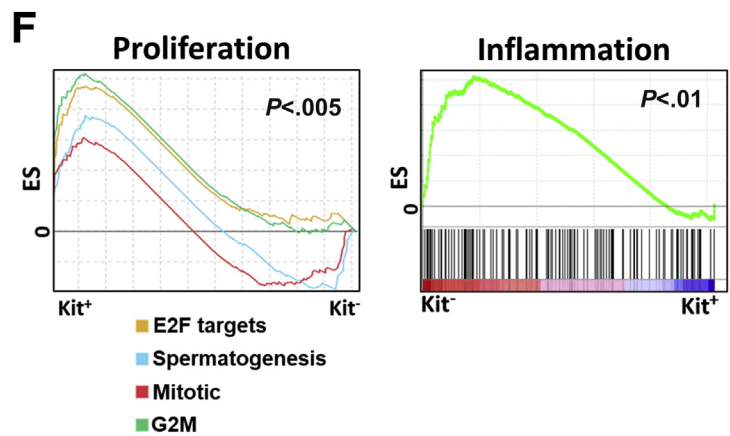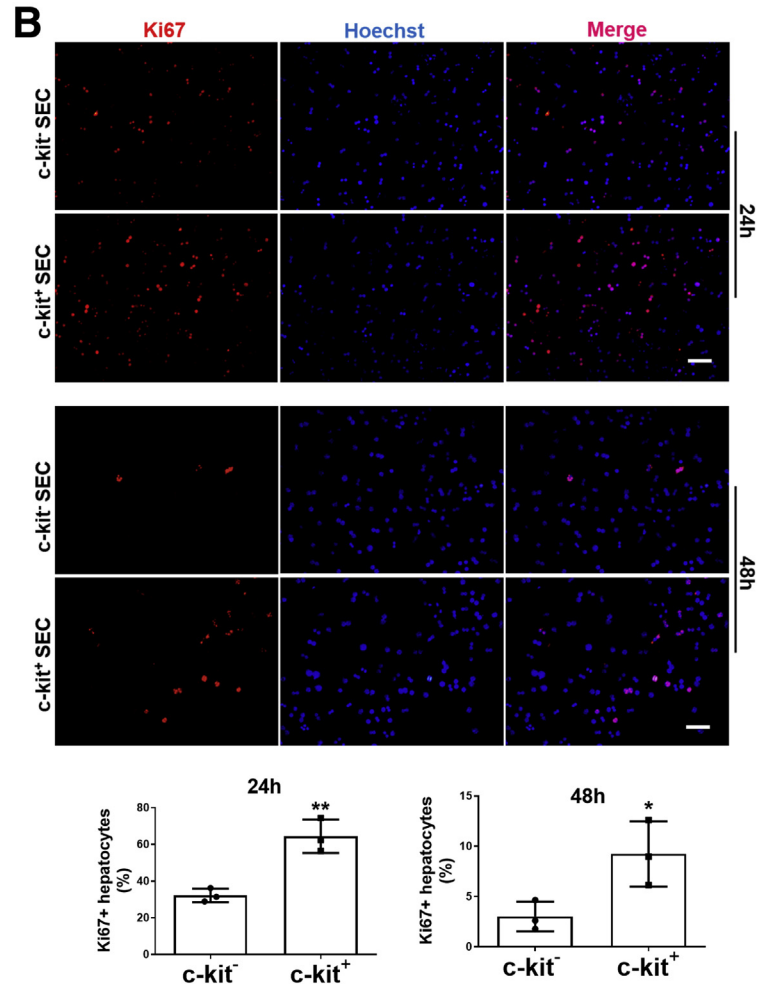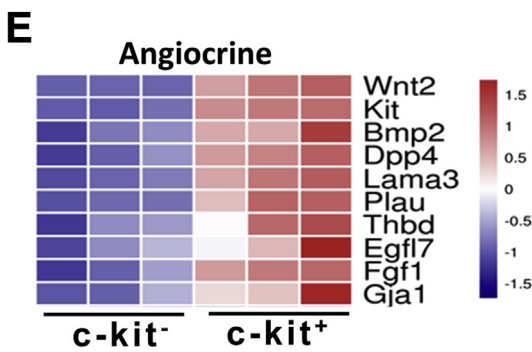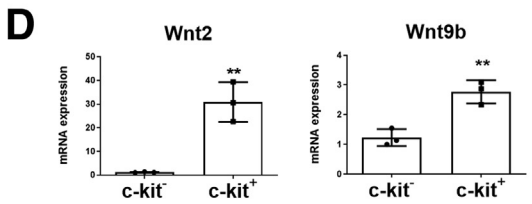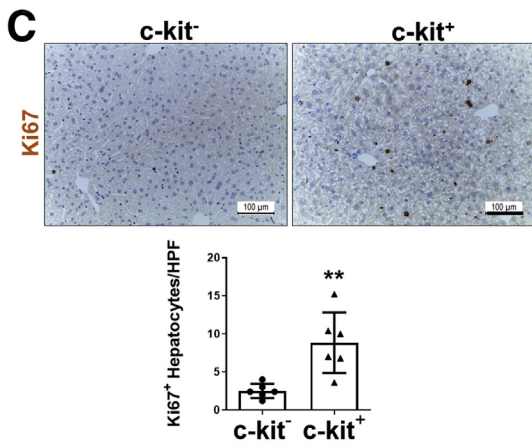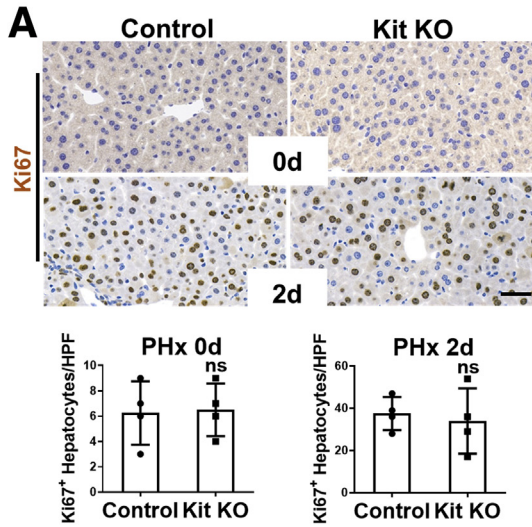
Moreover, tail vein infusion of c-kit$^+$ SECs successfully stimulated hepatocyte proliferation in vivo (Figure 3C). The expressions of Wnt2, Wnt9b, HGF, cyclinD1, and VEGFR1 were determined by quantitative reverse-transcription polymerase chain reaction (qRT-PCR). The results show that all of these angiocrine factors are highly expressed in c-kit$^+$ SECs (Figure 3D). To confirm the earlier-described findings, RNA-seq was performed on isolated SECs between c-kit$^+$ and c-kit$^-$ subpopulations. Consistently, the heatmap shows that angiocrine factors are up-regulated in c-kit$^+$ SECs (Figure 3E). Moreover, the gene set enrichment analyses unveiled that proliferation-related pathways including Early 2 factor targets, spermatogenesis, mitotic, and G2M were activated in c-kit$^+$ SECs, whereas inflammation-associated signaling was enriched in c-kit$^-$ SECs (Figure 3F). These data confirm our hypothesis that c-kit$^+$ SECs are devoted to supporting liver regeneration, probably in an angiocrine-dependent manner.

Single-cell RNA-Seq Shows Zonation-Like Distribution of Hepatic c-Kit

A recent study performed single-cell RNA-seq of murine global endothelial cells,[22] providing an atlas to observe molecular changes of endothelia in different organs. Based on this atlas, we found that c-kit was expressed only in the liver and lung endothelia (Figure 4A). In addition, hepatic c-kit could be detected only in liver endothelia, especially sinusoidal and central venous endothelial cells (Figure 4B and C), which was consistent with the findings obtained with single-cell RNA-seq (Figure 1A and B). The distribution of endothelial markers and angiocrine factors including Cdh5, Lyve1, CD146, VEGFR3, VEGFR2, VEGFR1, Wnt9b, HGF, and Wnt2 in liver endothelial cells are shown in Figure 4C as well. Interestingly, the spatial distribution of c-kit basically coincided with the liver zonation marker Wnt2. To confirm that the expression of Wnt2 is spatially highly correlated with c-kit, we used the databank of paired-cell sequencing of liver endothelial cells established by Halpern et al.[23]

The immunofluorescent staining shown in Figure 4D indicates high expression of hepatic c-kit around CV and low expression in PV areas. We delineate 8 continuous regions from PV to CV (Figure 4D) and estimate the spatial expression of several molecules in different regions of the liver by paired-cell sequencing (Figure 4E and F). We found that, from PV to CV, the expression of c-kit gradually increased in liver endothelial cells, which is consistent with the trend of Wnt2. The spatial expression levels of CXCR7, Wnt9b, and Myc are

roughly the same, in contrast to the changes in HGF, VEGFR1, and cyclin D1 (Figure 4E). Then, we measured the spatial expression of molecules related to the Notch signaling pathway and found that Notch1, Notch2, Notch4, Delta-like canonical Notch ligand 4, hairy/enhancer-of-split related with YRPW motif 1, and hes family bHLH transcription factor 1 showed spatial expression levels opposite to c-kit (Figure 4F). Thus, we speculate that hepatic c-kit and Wnt2 are regulated negatively by the Notch signaling pathway.

Notch Mutation Reshapes c-Kit Distribution and Liver Zonation, Affecting Hepatocyte Proliferation

To investigate whether Notch signaling is involved in the regulation of c-kit$^+$ SECs, we constructed Cdh5-Cre-ERT Notch intracellular domain (NICD) and Cdh5-Cre recombination signal binding protein Jκ (RBPj)^{floxp} mice, which were able to activate or abrogate endothelial Notch signaling, respectively. The heatmap of SEC RNA-seq shows that c-kit and Wnt2 are down-regulated in NICD overexpression mice, and up-regulated upon disruption of the endothelial Notch signal (Figure 5A). This was confirmed further by qRT-PCR (Figure 5B). In addition, immunofluorescent staining uncovered the spatial distribution of c-kit$^+$ SECs after the Notch mutation. c-Kit–positive signals were quantified in different regions marked zones 1–6 (Figure 5C and D). Forced Notch activation by NICD overexpression resulted in a large decrease of c-kit$^+$ SECs in midlobular (zones 2–3 and 4–5) and especially CV areas (zones 3–4) (Figure 5E and G). However, a sustainable increase of c-kit$^+$ SECs was found in all areas (zones 1–6) of the liver with Notch-RBPj deficiency (Figure 5F and H). A sketch made a summary that c-kit$^+$ SECs normally reside in CV or midlobular sinusoids. The spatial distribution of these c-kit$^+$ cells probably shift after Notch mutation (Figure 5I). Finally, immunohistochemistry staining with anti-Ki67 shows that the proliferation of hepatocytes decreases after Notch activation and increases after Notch disruption (Figure 5J). In summary, we presume that endothelial Notch signaling inhibits hepatocyte proliferation by regulating c-kit $^+$ SEC-derived Wnt2.

Endothelial Notch Activation Impedes Liver Regeneration by Abrogating c-Kit$^+$ SEC-Derived Wnt2

On day 2 after PHx, hepatocyte proliferation was disrupted by Notch activation (Figure 6A). alanine aminotransferase (ALT) and aspartate aminotransferase (AST)

Figure 3. (*See previous page*). **c-Kit$^+$ SECs promote hepatocyte proliferation in vivo and in vitro.** (*A*) Liver samples collected from control and Cdh5-Cre Kit^{floxp} mice on days 0 and 2 after PHx, analyzed with anti-Ki67 immunohistochemistry (IHC) (n = 4 per group). *Scale bar*: 50 μm. (*B*) Wild-type primary hepatocytes treated with the culture medium of c-kit$^+$ or c-kit$^-$ SECs in vitro. Twenty-four or 48 hours later, hepatocytes were collected and observed by Ki67 (red) and Hoechst (blue) co-stain. Ki67$^+$ hepatocytes (pink) were compared between the c-kit$^+$ and c-kit$^-$ groups (n = 3 per group). *Scale bars*: 50 μm. (*C*) Liver samples collected from normal mice 1 day after cell infusion. The proliferation of hepatocytes was compared between the groups infused with c-kit$^+$ or c-kit$^-$ SECs by anti-Ki67 IHC (n = 6 per group). *Scale bar*: 100 μm. (*D*) Expression of Wnt2, Wnt9b, HGF, cyclin D1, and VEGFR1 determined by qRT-PCR (n = 3 per group). (*E*) c-Kit$^+$ or c-kit$^-$ SECs isolated and analyzed by RNA-seq. The heatmap shows the change of some angiocrine factors. (*F*) Gene set enrichment analyses of isolated SECs between c-kit$^+$ and c-kit$^-$ groups. The enrichment of proliferation and inflammation-associated pathways were investigated. *Bars* show means ± SD. *$^*P$ < .05, **$^{**}P$ < .01, and ***$^{***}P$ < .001. KO, knockout.
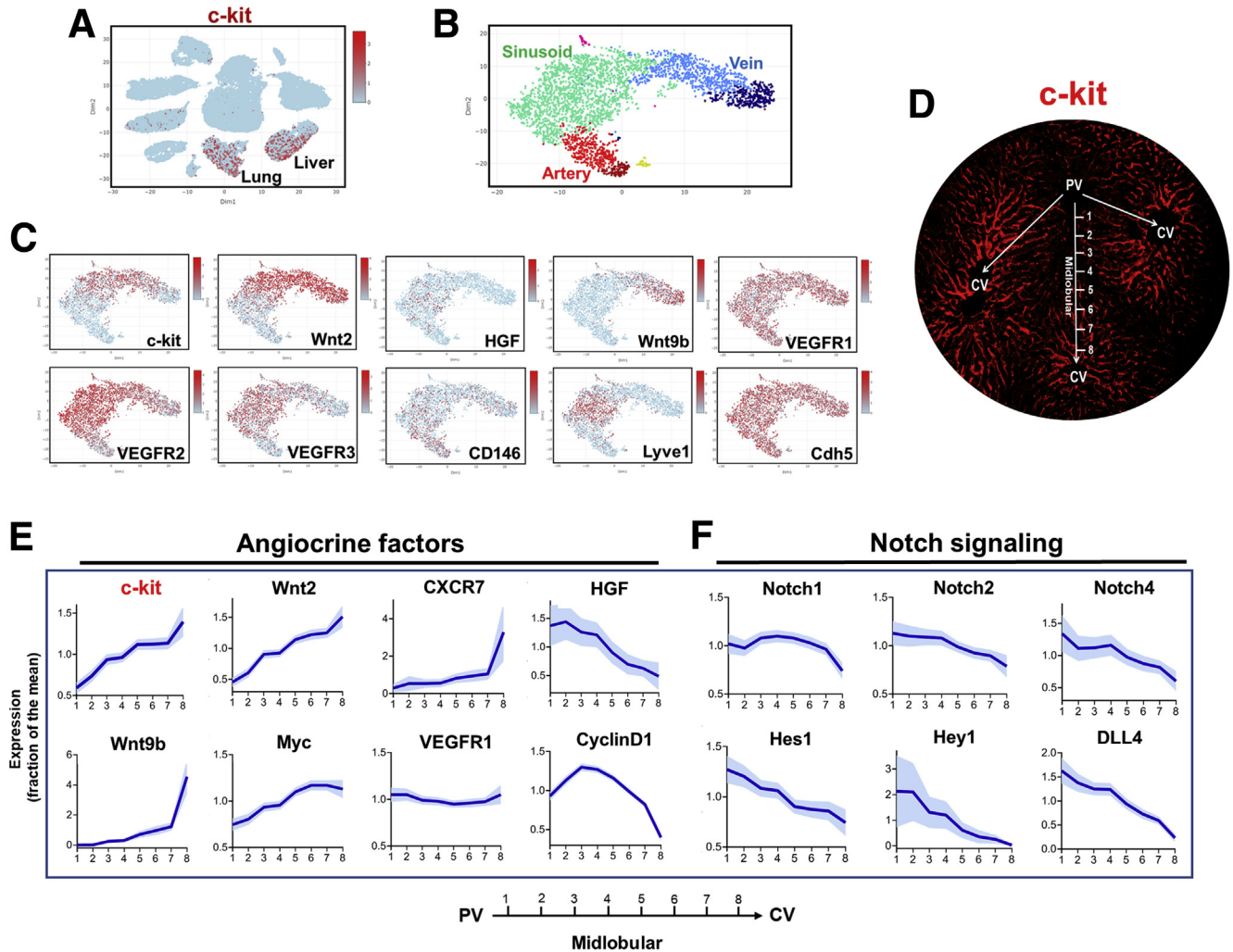
Figure 4. Spatial expression of hepatic c-kit, Wnt2, and Notch signaling. Single-cell RNA-seq showing (*A*) c-kit expression in murine global endothelial cells, (*B*) the cluster of liver endothelial cells, and (*C*) the expression of c-kit, Wnt2, HGF, Wnt9b, VEGFR1, VEFGR2, VEGFR3, CD146, Lyve1, and Cdh5 in liver endothelial cells. (*D*) Normal liver section stained with c-kit (red) and factitiously divided into 8 continuous regions from the PV to CV. (*E* and *F*) Spatial expression of angiocrine factors and Notch signaling genes presented by paired-cell sequencing.

increased significantly, and the liver/body weight ratio decreased 2 days after PHx (Figure 6*B* and *C*), suggesting that NICD overexpression impaired liver regeneration and deteriorated liver function. c-Kit⁺ SECs then were calculated by FACS. Compared with the control, Notch activation strikingly reduced the c-kit⁺ SEC population (Figure 6*D*). To determine whether Notch impaired liver regeneration occurs as a result of the loss of c-kit⁺ SECs, we isolated normal c-kit⁺ SECs and infused them in PHx models. Immunohistochemistry staining with anti-Ki67 showed that incapable hepatocyte proliferation caused by Notch activation was recovered by c-kit⁺ SEC infusion (Figure 6*E* and *F*). Although reduced liver weight was not affected, impaired liver function by Notch activation was restored after cell infusion (Figure 6*G* and *H*). Considering that c-kit⁺ SECs were rich in Wnt2 expression, we examined the Wnt2 mRNA level after PHx and Notch activation. qRT-PCR showed that Wnt2 was highly expressed in c-kit⁺

SECs of the regenerating liver (Figure 6*I*). After Notch activation, Wnt2 showed a significantly larger decrease in the c-kit⁺ than in the c-kit⁻ group (Figure 6*J*). To evaluate the contribution of Wnt2 to regeneration, c-kit⁺ SECs with different genotypes were isolated and cocultured with primary hepatocytes of wild-type mice. The addition of exogenous Wnt2 plasmid in vitro rescues the disrupted hepatocyte proliferation caused by Notch activation (Figure 6*K*). In summary, the Notch signal influences c-kit⁺ SECs to regulate liver regeneration in a Wnt2-dependent manner.

c-Kit⁺ SEC Infusion Ameliorates Liver Injury

Considering that c-kit⁺ SECs have the capacity to promote hepatocyte regeneration, we further identified their therapeutic potential on liver injuries. Liver injury models were established by CCl₄ or qPCR (DMN). In both models,
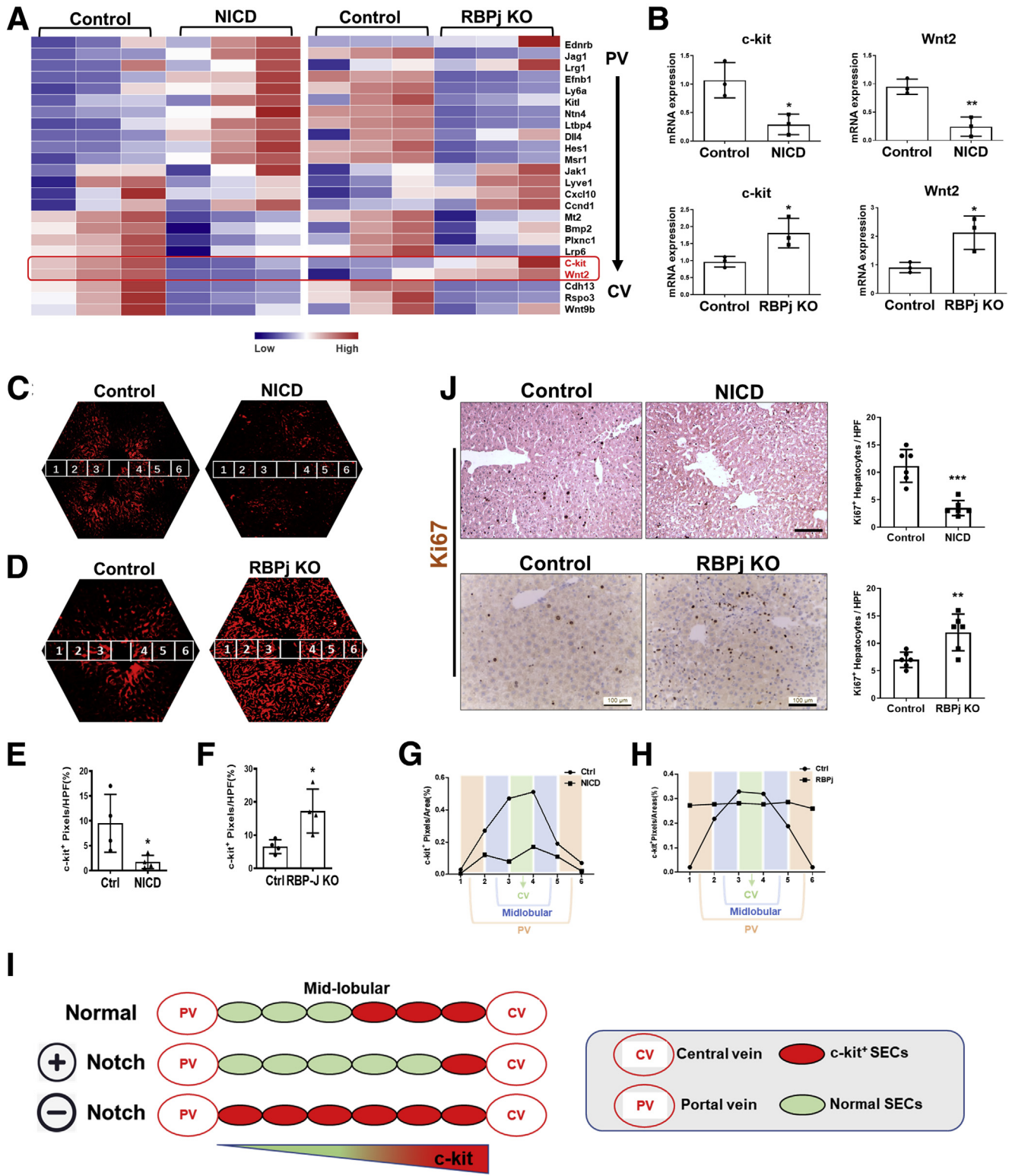
Figure 5. Notch mutation reshaped c-kit distribution and altered hepatocyte proliferation. (*A*) Heat map showing the gene profiles of SECs collected from the control, NICD overexpression, and RBPj knockout mice. The *P* value of each comparison is indicated with colors. (*B*) qRT-PCR comparison of c-kit and Wnt2 expression levels between the control and NICD mice or the control and RBPj KO mice (n = 3 per group). (*C* and *D*) Liver sections collected from the control and Notch mutant mice stained with c-kit (red) and then factitiously divided into 6 continuous regions. (*E* and *F*) Quantification of c-kit staining shown in panels *C* and *D* (n = 4 per group). (*G* and *H*) Relative distribution of c-kit in different regions (1–6) of liver estimated according to the c-kit stain shown in panels *C* and *D* (n = 4 per group). (*I*) Sketch imitating the spatial expression of hepatic c-kit among the normal control, NICD, and RBPj KO groups. (*J*) Liver samples collected from the control, NICD overexpression, and RBPj KO mice and analyzed by anti-Ki67 immunohistochemistry (n = 5–6 per group). *Scale bars*: 100 μm. *Bars* show means ± SD. *$P <$ .05, **$P <$ .01, and ***$P <$ .001. HFP, high-power field.
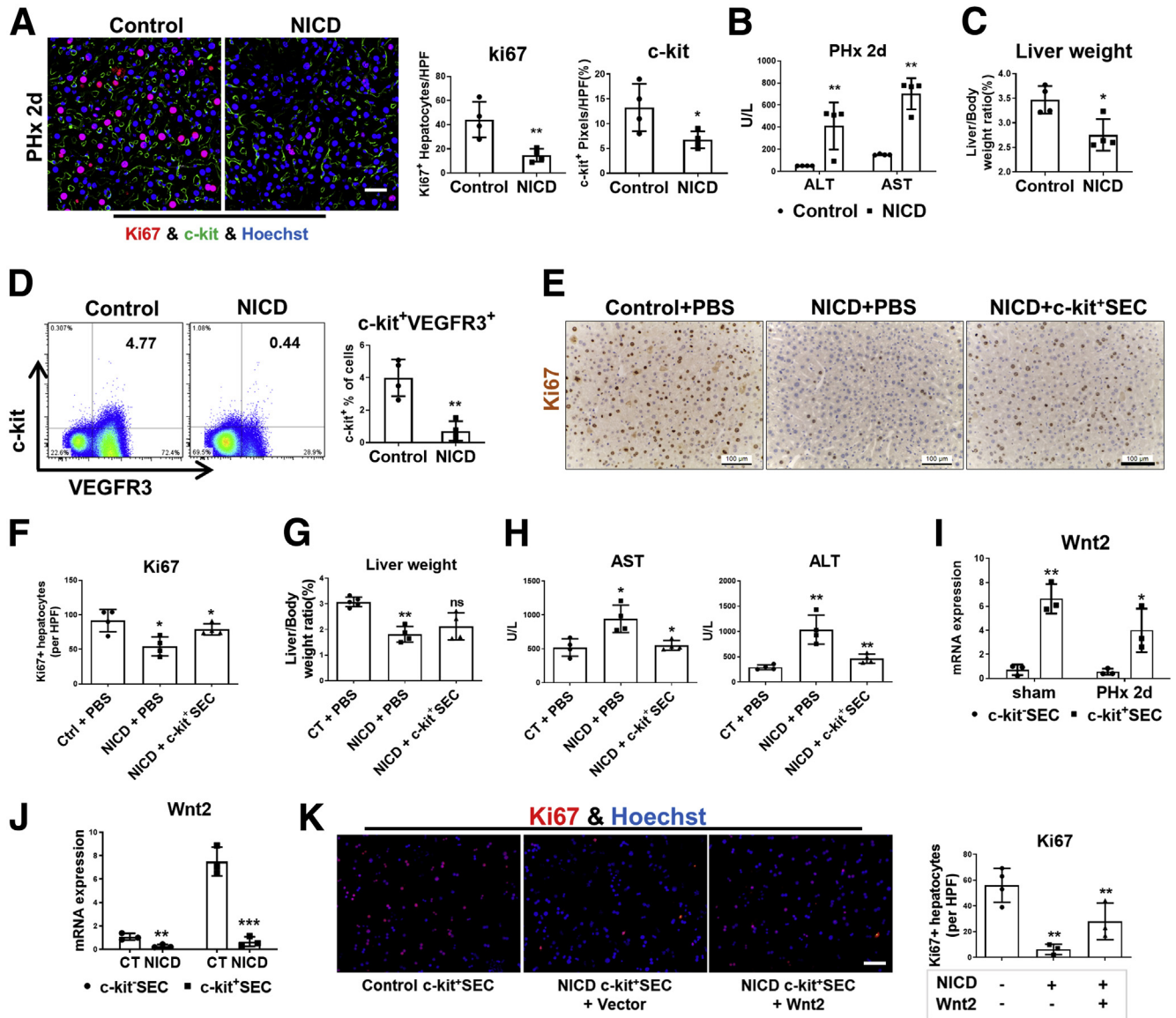
Figure 6. Endothelial Notch activation impairs liver regeneration by disrupting c-kit$^+$ SEC-derived Wnt2 angiocrine. (*A*) Liver sections collected from the control and NICD overexpressed mice co-stained with Ki67 (red), c-kit (green), and Hoechst (blue) on PHx day 2. Ki67$^+$ nuclei of hepatocytes (pink) and c-kit expression were quantified (n = 4 per group). *Scale bar*: 50 μm. (*B* and *C*) Serum levels of ALT and AST and the liver/body weight ratio were compared between the control and NICD mice on day 2 after PHx (n = 4 per group). (*D*) c-Kit$^+$ and VEGFR3$^+$ liver cells measured and quantified by FACS in the control and NICD-overexpressed mice (n = 4 per group). (*E*) Mice with different genotypes were infused with phosphate-buffered saline (PBS) or c-kit$^+$ SECs twice on PHx days 0 and 1. *Scale bars*: 100 μm. (*F*) Proliferating hepatocytes were labeled by anti-Ki67 immunohistochemistry and quantified (n = 4 per group). (*G* and *H*) Relative liver weight, ALT, and AST were compared among the control group with PBS infusion, NICD group with PBS infusion, and NICD group with c-kit$^+$ SEC infusion (n = 4–5 per group). (*I* and *J*) Expression of Wnt2 was compared between c-kit$^+$ and c-kit$^-$ SECs by qRT-PCR, after PHx or endothelial Notch activation (n = 3 per group). (*K*) Hepatocytes isolated from wild-type mice were treated with the culture medium of c-kit$^+$ SECs in control, NICD, or NICD with Wnt2 overexpression group. The proliferation of hepatocytes was analyzed and quantified by Ki67 (red) stain (n = 3–4 per group). *Scale bar*: 50 μm. *Bars* show means ± SD. *$P <$ .05, **$P <$ .01, and ***$P <$ .001. Ctrl, control; CT, control; HPF, high-power field.

wild-type mice were implanted with c-kit$^+$ or c-kit$^-$ SECs through the spleen 12 hours after CCl$_4$ or DMN administration and were analyzed 36 hours after cell infusion. To verify whether the implanted SECs successfully could home to the liver, GFP-labeled c-kit$^+$ SECs were detected by immunofluorescent stain. As shown in Figure 7*M*, GFP-

positive stain could be notably observed in both groups. In CCl$_4$-induced models, the liver with c-kit$^+$ SEC infusion seemed normal; however, the control liver infused with c-kit$^-$ SECs was reddish, indicating that CCl$_4$ leads to liver congestion (Figure 7*A*). Although the relative liver weight and ALT level remained unchanged after cell infusion
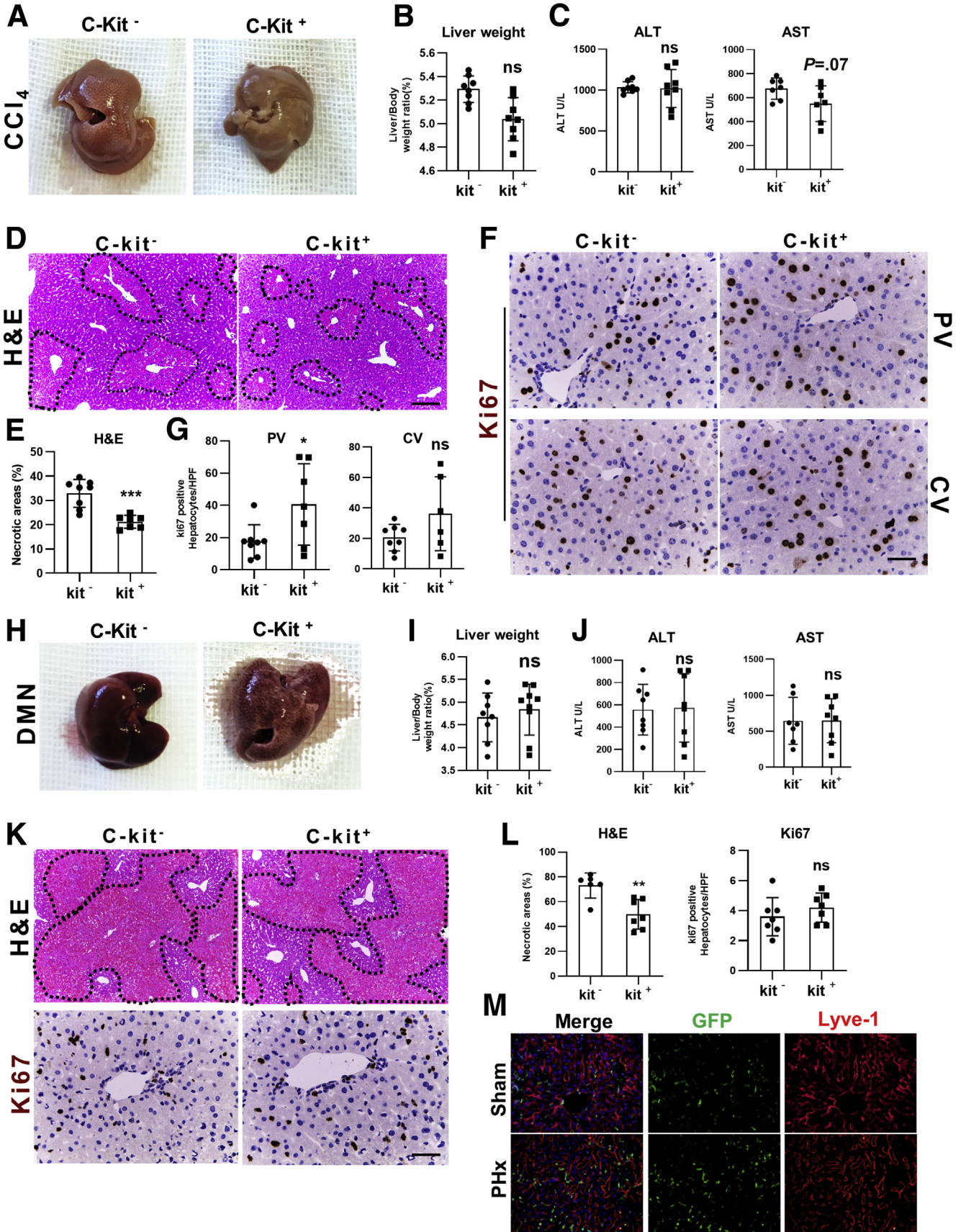
(Figure 7B and C), c-kit$^+$ SECs alleviated liver injury by decreasing the AST level (Figure 7C) and decreasing liver necrotic areas shown by H&E staining (Figure 7D and E). Furthermore, c-kit$^+$ SEC infusion promoted periportal hepatocyte proliferation after CCl$_4$ injury (Figure 7F and G). In DMN-induced models, c-kit$^+$ SEC infusion largely ameliorated liver congestion in general (Figure 7H). Although the liver weight, ALT, AST, and hepatocyte proliferation were not affected significantly by cell infusion, H&E staining showed that c-kit$^+$ SECs improved liver necrosis after DMN injection (Figure 7I–L). These findings indicate the potential therapeutic role of c-kit$^+$ SECs in toxin-induced liver injuries.

Discussion

In this study, c-kit$^+$ SECs first were identified as a contributor to the liver regeneration process. c-Kit, also known as CD117, has been referred to as the SCF receptor. Activation of the SCF/c-kit signal transduction pathway usually is linked to cell proliferation, migration, and survival, and thus regulates crucial functions in hematopoiesis, pigmentation, and spermatogenesis. Interestingly, in this study, we found that c-kit was largely expressed in SECs. Notably, we provide evidence showing c-kit$^+$ SECs are rich in terms of angiocrine factor expression, which suggests that c-kit$^+$ SECs produce predominant mitogens during liver regeneration. Liver c-kit$^+$ cells, including some hepatocytes, Biliary epithelial cells, and oval cells, have been proposed to participate in liver regeneration by differentiating into different types of cells, depending on the type of the injury.[24–26] Some research groups showed that bone marrow c-kit$^+$ cells repopulated to the liver and attenuated hepatocyte damage by differentiating into NPCs or secreting protective cytokines.[27,28] However, bone marrow transplant and parabiosis models confirmed that circulating c-kit$^+$ cells contributed less to PHx-induced c-kit increase than expected. Compared with the circulating c-kit$^+$ cells, we presumed that the resident c-kit$^+$ SECs provide a quick response and become the main source of angiocrine factors during liver regeneration. The cell biology and specific regulation of circulating bone marrow c-kit$^+$ cells during liver injury will be explored in subsequent work.

Hepatocytes with different characteristics and functions are distributed unevenly along the radial axis of the lobule, termed the *zonation*.[5–7] Liver zonation, the spatial separation of different metabolic pathways along the liver sinusoids, is fundamental for proper functioning of this organ. The Wnt signaling pathway is considered to be the main regulator of liver zonation.[8] Its activity is highest around the central vein, and nuclear β-catenin directly regulates the activation of genes involved in glutamine synthesis and drug metabolism. The genes expressed near central vein endothelial cells are the key ligands of the Wnt signaling pathway, including Wnt2, Wnt9b, and Rspo3.[8] Recently, Inverso et al[29] and Su et al[30] unveiled that the SEC-derived c-kit contributed to liver zonation in the quiescent or fibrotic liver. Consistently, by analyzing the single-cell sequencing database,[23] the spatial distribution of c-kit$^+$ SECs is zonation-like in the liver, which is consistent with the Wnt2 expression, further implicating that c-kit$^+$ SECs may be responsible for hepatocyte proliferation by the angiocrine pathway in liver regeneration.

According to RNA-seq and the immunofluorescent stain of the Notch signal expression pattern in our study, Notch signaling negatively regulates the spatial expression of hepatic c-kit and Wnt2. We previously showed that endothelial Notch activation results in SEC dedifferentiation and alters the angiocrine profile of SECs to compromise hepatocyte proliferation and liver regeneration.[4] Herein, we elucidate whether c-kit$^+$ SECs also could be regulated by Notch signaling. After forced activation of the Notch signaling pathway, the number of c-kit$^+$ SECs decreased, and Wnt2 was down-regulated in c-kit$^+$ SECs. The influx of c-kit$^+$ SECs in vivo and exogenous overexpression of Wnt2 in vitro confirmed that the Notch signaling pathway manipulated hepatocyte proliferation by regulating c-kit$^+$ SEC-derived Wnt2. We also found that some other angiocrine factors, such as CXCR7, Wnt9b, HGF, and cyclin D1 were highly expressed in c-kit$^+$ SECs. Whether these angiocrine factors also are regulated strictly by Notch signaling pathways must be addressed in future work. The endothelial NICD overexpression shrank c-kit$^+$ SECs. Whether Notch-Hes1 signaling directly impedes the c-kit transcription or disrupts the c-kit in some other ways also must be explored in a subsequent study.

In this study, we showed that c-kit$^+$ SECs have potential therapeutic effects on the treatment of liver injuries, probably by promoting hepatocyte regeneration. We assume that exogenous c-kit$^+$ SECs may act as Trojan horses that provide certain angiocrine factors, such as Wnt2, to fuel hepatocyte proliferation. The RNA-seq analysis of isolated SECs confirms that the proliferation-associated signaling pathways including Early 2 factor targets, spermatogenesis, mitotic, and G2M, are activated extensively in c-kit$^+$ instead of c-kit$^-$ SECs, indicating c-kit$^+$ SECs were the major source of mitogens that stimulated hepatocyte proliferation and recovered the injured liver. These findings imply that c-kit$^+$ SECs may become candidate cells for the treatment of liver diseases in the future. However, the potential value of c-kit$^+$ SECs in the field of liver repair and disease treatment and its therapeutic mechanism require further investigation.

Figure 7. (*See previous page*). **c-Kit$^+$ SEC infusion recovers injured liver.** Wild-type mice were implanted with c-kit$^+$ or c-kit$^-$ SECs through the spleen 12 hours after CCl$_4$ or DMN administration and analyzed 36 hours after cell infusion. (*A and H*) CCl$_4$-or DMN-treated liver after c-kit$^+$ or c-kit$^-$ SEC infusion. (*B and I*) Liver/body weight ratio of mice with liver injury and cell infusion (n = 8–9 per group). (*C and J*) Serum ALT and AST levels of mice with liver injury and cell infusion (n = 7–8 per group). (*D, F, and K*) H&E staining and anti-Ki67 immunohistochemistry staining of injured liver after c-kit$^+$ or c-kit$^-$ SEC infusion. *Scale bars*: 100 μm. (*E, G, and L*) Quantification of liver necrotic areas and Ki67$^+$ hepatocytes shown in panels *D, F, and K* (n = 6–8 per group). (*M*) Implanted GFP-labeled SECs that were co-stained with Lyve-1 (red), were evaluated by immunofluorescent stain in the liver of PHx and control mice. *Bars* show means ± SD. *P < .05, **P < .01, and ***P < .001.
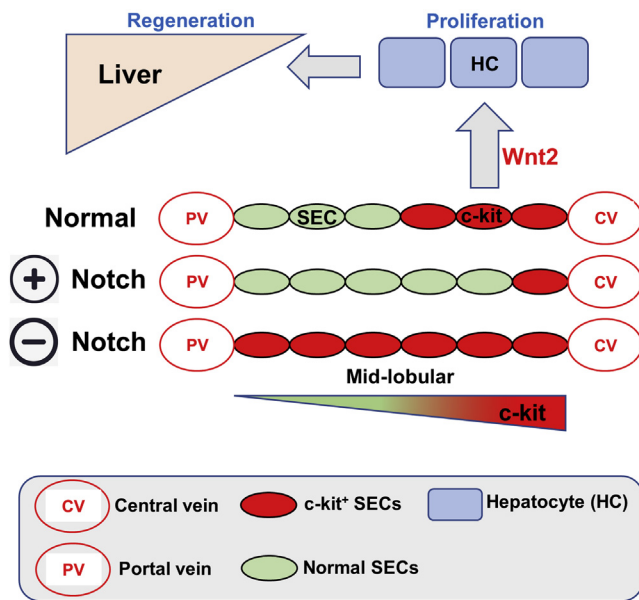
Figure 8. Graphic summary. Schematic showing regulatory effects of Notch signaling on c-kit$^+$ SECs.

In summary, our data show that c-kit$^+$ SECs, a newly identified SEC subtype, contribute to liver regeneration via angiocrine factors. The angiocrine property of c-kit$^+$ SECs is dysregulated by Notch signal activation and compromises hepatocyte proliferation (Figure 8). The results provide promise for elucidating the mechanism of c-kit$^+$ SEC-mediated hepatocyte proliferation in liver regeneration and propose that targeting c-kit$^+$ SEC may be an attractive rationale for treating liver disease.

Materials and Methods

Mice

Mice were maintained in a specific pathogen-free facility on the background of C57BL/6J. Gt(ROSA)26Sor Harbor site-transcription stop signal^{floxed}-Notch1 intracellular domain-mice (murine Notch1 NIC [1749-2293], followed by the internal ribosome entry site-GFP in the ROSA26 locus; Jackson Laboratory, Bar Harbor, ME) were crossed with CDH5-Cre-ERT mice (kindly provided by R.H. Adams).[31] Male mice (6 weeks old) were injected intraperitoneally with tamoxifen (100 mg/kg; Sigma Aldrich, St. Louis, MO), 7 times in total.[32] The RBP-J–floxed mouse strain was constructed as described.[33] The Cdh5-Cre Kit^{floxp} mice were constructed by GemPharmatech Co, Ltd (Nanjing, China).

PHx was performed as described.[34] To induce liver injury, mice were injected with CCl_4 (15% in olive oil, 0.6 mL/g body weight, intraperitoneally) or DMN (dissolved in olive oil, 14 mg/kg body weight, intraperitoneally). For cell infusion, 2×10^6 c-kit$^+$ SECs were collected by magnetic sorting and injected via the tail vein or spleen.

All animal experiments were approved by the Animal Experiment Administration Committee of the Fourth Military Medical University (Xi'an, China) to ensure ethnical and humane treatment of animals. The study was performed according to the guidelines outlined in the National Institutes of Health Guide for the Care and Use of Laboratory Animals prepared by the National Academy of Science and published by the National Institutes of Health (publication 86-23, revised 1985).

Bone Marrow Transplantation

C57BL/6 male mice at the age of 6–8 weeks were maintained under specific-pathogen-free conditions. Mice were subjected to total body irradiation, with γ-radiation from a ^{60}Co irradiator at a dosage of 9 Gy. Then, mice were injected with BM cells through the tail vein.[35]

Parabiosis Models

The mice to be joined in parabiosis were anesthetized by inhaled isoflurane, 2.0%–3.0% vol/vol induction, 1.5%–2.0% vol/vol maintenance. The mice were placed in the supine position, fur was removed from the surgical site, and excess hair was wiped off with an alcohol swab. After further disinfection, incisions were made starting at 0.5 cm above the elbow all the way to 0.5 cm below the knee joint, attaching

Table 1. Antibodies Used in This Study

Name	Supplier	Clone number	Purpose
c-kit	R&D Systems (Minneapolis, MN)	Polyclonal	FACS/IF
VEGFR2	Abcam (Cambridge, UK)	Monoclonal	FACS
Lyve-1	Reliatech (Brunswick, Germany)	4D17	IF
CD146	Biolegend (San Diego, CA)	ME-9F1	FACS
CD31	Biolegend (San Diego, CA)	MEC13.3	FACS/IF
VEGFR3	Abcam (Cambridge, UK)	Monoclonal	FACS
CD45	Abcam (Cambridge, UK)	Monoclonal	FACS
Ki67	Millipore (Burlington, MA)	Polyclonal	IF/IHC
Goat anti-rabbit FITC	Jackson Immuno Research (Pennsylvania, PA)	IgG	IF
Goat anti-rabbit Cy3	Jackson Immuno Research (Pennsylvania, PA)	IgG	IF
Donkey anti-goat Alexa fluo594	LifeTechnologies (Carlsbad, CA)	IgG	IF

FITC, fluorescein isothiocyanate; IF, immunofluorescence; IHC, immunohistochemistry.

Table 2. Primers Used for qPCR

qPCR	Forward, 5'-3'	Reverse, 5'-3'
c-kit	GCCACGTCTCAGCCATCTG	GCCACGTCTCAGCCATCTG
CXCR7	TAAGACCACAGGCTACGACA	TGAGGTGTGTGATCTTGCATG
HGF	CCGACGAGACCGAATCAATAAC	CGTCCCTTTATAGCTGCCTCC
CD31	AGTCAGAGTCTTCCTTGCCC	TCTGTTTGGCCTTGGCTTTC
Wnt2	CTCGGTGGAATCTGGCTCTG	CACATTGTCACACATCACCCT
Angpt2	AGAAGAGCAAACCACCTTCAG	GTCACAGTAGGCCTTGATCTCC
VEGFR1	TGGCTCTACGACCTTAGACTG	CAGGTTTGACTTGTCTGAGGTT
VEGFR2	TTTGGCAAATACAACCCTTCAG	GCAGAAGATACTGTCACCACC
VEGFR3	CTGGCAAATGGTTACTCCATGA	ACAACCCGTGTGTCTTCACTG
CD146	CCTGGAACGTCAACGGCAC	GGGTGGTTAAATTGACCAGCTCC
Tie2	CATCACCATAGGAAGGGAC	CACGGTCATAGTTAGAGTAGCA
Cdh5	ATTGGATTTGGAACCAGATGC	ACGCTTGACTTGATCTTGC
Wnt9b	CTGGTGCTCACCTGAAGCAG	CCGTCTCCTTAAAGCCTCTCTG
CyclinD1	GCGTACCCTGACACCAATCTC	CTCCTCTTCGCACTTCTGCTC
β-actin	GGCTGTATTCCCCTCCATCG	CCAGTTGGTAACAATGCCATG

the left olecranon/knee joint of one mouse to the right olecranon/knee joint of the other. The olecranon and knee joints were each attached tightly by a double surgical knot. Then, the dorsal and ventral skins were connected with a continuous 5-0 Vicryl (Shanghai, China) suture. The mice were kept on a heated pad and continuously monitored until complete recovery.[36]

Histologic Examination

Paraffin-embedded and snap-frozen liver sections were prepared for immunohistochemistry and immunofluorescence according to standard protocols. Cultured SECs were grown on cover slides in 24-well plates for the indicated number of days and then processed for in vitro immunofluorescence. Antibodies used for histology are listed in Table 1. In situ hybridization was performed as described in a previous study.[37] Scanning electron microscopy was performed as described in a previous study.[4] Fluorescein isothiocyanate/formaldehyde-treated serum albumin was used to assay the endocytosis of SECs in vivo, as instructed by published protocols.[38]

c-Kit^{+/-} SEC Isolation

Cells were isolated as described in a previous study.[4] Briefly, mice were anesthetized and perfused with Hank's buffer containing 0.2 mg/mL of collagenase IV (Sigma-Aldrich). Hepatocytes were removed by low-speed centrifugation at $50 \times g$ for 3 minutes. Liver NPCs were resuspended in 4 mL of 17.6% iodixanol (Axis-Shield, Dundee, Scotland) and 4 mL of 10% iodixanol. The cell suspension then was centrifuged at $1400 \times g$ for 20 minutes in a swing-out rotor without brake. Cells were recovered from the interface between the 10% and 17.6% iodixanol solutions, and resuspended and incubated with anti-CD117 magnetic beads (Miltenyi Biotec) for 15 minutes in the dark in the refrigerator. By magnetic separation with MS Columns (Bergisch Gladbach, Germany), c-kit^{+} cells were collected by

pushing the plunger into the MS column. The eluted fraction can be enriched and incubated with anti-CD146 magnetic beads, upon which magnetic separation obtains the c-kit^{-} cells.

Flow Cytometry

Single-cell suspensions were incubated with the indicated antibodies (listed in Table 1) in the flow cytometry staining buffer (eBioscience, San Diego, CA) for 30 minutes, followed by staining with fluorescent secondary antibody when necessary. Samples were analyzed with a FC500 flow cytometer (Beckman, Brea, CA), and data were analyzed using FlowJo 7.6 software. Unstained cells were used for determining gates, and isotype antibodies were used for negative control.

Single-Cell RNA-Seq

Single-cell RNA-seq was performed as previously described,[39] and was supported by the Genergy Biotechnology (Shanghai, China). Hepatic NPCs were collected and loaded on a Chromium Single Cell Instrument (Pleasanton, CA) ($10\times$ genomics) to generate single-cell barcoded droplets (Gel Bead-In-EMulsions) according to the manufacturer's protocol. Sequencing was performed on an Illumina HiSeq3000 (San Diego, CA). Raw data files of single-cell RNA-seq in this study are accessible through GEO (accession number: GSE134037).

RT-PCR

Total RNA was extracted from cells or total liver tissue using the TRIzol reagent (Invitrogen, Carlsbad, CA) according to the manufacturer's instructions. After reverse-transcription using a PrimeScrip RT reagent kit (Takara, Dalian, China), qPCR was performed with the SYBR Premix EX Taq II kit (Takara) on an ABI 7500 real-time PCR system

(Applied Biosystems, Foster City, CA), with β-actin as an internal control. The primers used are listed in Table 2.

Biochemical Detection

Serum levels of ALT and AST were analyzed using kits (BioSino Bio-Technology and Science, Inc, Beijing, China) and an automatic biochemistry analyzer (Chemray240; Rayto, Shenzhen, China). The hydroxyproline content was quantified using a kit (Sigma-Aldrich) according to the manufacturer's instruction.

Statistical Analysis

The SPSS (version 12.0; SPSS, Inc, Chicago, IL) program was used to perform statistical analysis. An unpaired t test or analysis of variance were performed to compare the difference between each group. Results are expressed as means $\pm$ SD. $P < .05$ was considered statistically significant.

References

1. Ozaki M. Cellular and molecular mechanisms of liver regeneration: proliferation, growth, death and protection of hepatocytes. Semin Cell Dev Biol 2020;100:62–73.
2. Miyajima A, Tanaka M, Itoh T. Stem/progenitor cells in liver development, homeostasis, regeneration, and reprogramming. Cell Stem Cell 2014;14:561–574.
3. Duncan AW, Soto-Gutierrez A. Liver repopulation and regeneration: new approaches to old questions. Curr Opin Organ Transplant 2013;18:197–202.
4. Duan JL, Ruan B, Yan XC, Liang L, Song P, Yang ZY, Liu Y, Dou KF, Han H, Wang L. Endothelial Notch activation reshapes the angiocrine of sinusoidal endothelia to aggravate liver fibrosis and blunt regeneration in mice. Hepatology 2018;68:677–690.
5. Manco R, Itzkovitz S. Liver zonation. J Hepatol 2021; 74:466–468.
6. Felmlee DJ, Grün D, Baumert TF. Zooming in on liver zonation. Hepatology 2018;67:784–787.
7. Leibing T, Géraud C, Augustin I, Boutros M, Augustin HG, Okun JG, Langhans CD, Zierow J, Wohlfeil SA, Olsavszky V, Schledzewski K, Goerdt S, Koch PS. Angiocrine Wnt signaling controls liver growth and metabolic maturation in mice. Hepatology 2018; 68:707–722.
8. Perugorria MJ, Olaizola P, Labiano I, Esparza-Baquer A, Marzioni M, Marin JJG, Bujanda L, Banales JM. Wnt-β-catenin signalling in liver development, health and disease. Nat Rev Gastroenterol Hepatol 2019;16:121–136.
9. Wakabayashi T, Naito H, Suehiro JI, Lin Y, Kawaji H, Iba T, Kouno T, Ishikawa-Kato S, Furuno M, Takara K, Muramatsu F, Weizhen J, Kidoya H, Ishihara K, Hayashizaki Y, Nishida K, Yoder MC, Takakura N. CD157 marks tissue-resident endothelial stem cells with homeostatic and regenerative properties. Cell Stem Cell 2018; 22:384–397.e6.
10. Ding BS, Nolan DJ, Butler JM, James D, Babazadeh AO, Rosenwaks Z, Mittal V, Kobayashi H, Shido K, Lyden D, Sato TN, Rabbany SY, Rafii S. Inductive angiocrine signals from sinusoidal endothelium are required for liver regeneration. Nature 2010;468:310–315.
11. LeCouter J, Moritz DR, Li B, Phillips GL, Liang XH, Gerber HP, Hillan KJ, Ferrara N. Angiogenesis-independent endothelial protection of liver: role of VEGFR-1. Science 2003;299:890–893.
12. Ding BS, Cao Z, Lis R, Nolan DJ, Guo P, Simons M, Penfold ME, Shido K, Rabbany SY, Rafii S. Divergent angiocrine signals from vascular niche balance liver regeneration and fibrosis. Nature 2014;505:97–102.
13. Hu J, Srivastava K, Wieland M, Runge A, Mogler C, Besemfelder E, Terhardt D, Vogel MJ, Cao L, Korn C, Bartels S, Thomas M, Augustin HG. Endothelial cell-derived angiopoietin-2 controls liver regeneration as a spatiotemporal rheostat. Science 2014;343:416–419.
14. Winkler M, Staniczek T, Kürschner SW, Schmid CD, Schönhaber H, Cordero J, Kessler L, Mathes A, Sticht C, Neßling M, Uvarovskii A, Anders S, Zhang XJ, von Figura G, Hartmann D, Mogler C, Dobreva G, Schledzewski K, Géraud C, Koch PS, Goerdt S. Endothelial GATA4 controls liver fibrosis and regeneration by preventing a pathogenic switch in angiocrine signaling. J Hepatol 2021;74:380–393.
15. Fujio K, Hu Z, Evarts RP, Marsden ER, Niu CH, Thorgeirsson SS. Coexpression of stem cell factor and c-kit in embryonic and adult liver. Exp Cell Res 1996; 224:243–250.
16. Zhou F, Li X, Wang W, Zhu P, Zhou J, He W, Ding M, Xiong F, Zheng X, Li Z, Ni Y, Mu X, Wen L, Cheng T, Lan Y, Yuan W, Tang F, Liu B. Tracing haematopoietic stem cell formation at single-cell resolution. Nature 2016;533:487–492.
17. Yushkov BG, Danilova IG, Ponezheva Zh B, Brykina IA, Abidov MT, Kalyuzhin OV. Modulation of reparative regeneration and CD117 expression by liver cells after partial hepatectomy in mice. Bull Exp Biol Med 2011; 150:352–354.
18. Weiskirchen R, Meurer SK, Liedtke C, Huber M. Mast cells in liver fibrogenesis. Cells 2019;8:1429.
19. Kennedy L, Meadows V, Sybenga A, Demieville J, Chen L, Hargrove L, Ekser B, Dar W, Ceci L, Kundu D, Kyritsi K, Pham L, Zhou T, Glaser S, Meng F, Alpini G, Francis H. Mast cells promote non-alcoholic fatty liver disease phenotypes and microvesicular steatosis in mice fed Western diet. Hepatology 2021;74:164–182.
20. Ren X, Carpenter A, Hogaboam C, Colletti L. Mitogenic properties of endogenous and pharmacological doses of macrophage inflammatory protein-2 after 70% hepatectomy in the mouse. Am J Pathol 2003;163:563–570.
21. Meng F, Francis H, Glaser S, Han Y, DeMorrow S, Stokes A, Staloch D, Venter J, White M, Ueno Y, Reid LM, Alpini G. Role of stem cell factor and granulocyte colony-stimulating factor in remodeling during liver regeneration. Hepatology 2012;55:209–221.
22. Kalucka J, de Rooij LPMH, Goveia J, Rohlenova K, Dumas SJ, Meta E, Conchinha NV, Taverna F, Teuwen LA, Veys K, García-Caballero M, Khan S, Geldhof V, Sokol L, Chen R, Treps L, Borri M, de Zeeuw P, Dubois C, Karakach TK, Falkenberg KD, Parys M, Yin X, Vinckier S, Du Y, Fenton RA, Schoonjans L, Dewerchin M, Eelen G, Thienpont B, Lin L, Bolund L, Li X, Luo Y,

Carmeliet P. Single-cell transcriptome atlas of murine endothelial cells. Cell 2020;180:764–779.e20.

23. Halpern KB, Shenhav R, Massalha H, Toth B, Egozi A, Massasa EE, Medgalia C, David E, Giladi A, Moor AE, Porat Z, Amit I, Itzkovitz S. Paired-cell sequencing enables spatial gene expression mapping of liver endothelial cells. Nat Biotechnol 2018;36:962–970.

24. van Berlo JH, Kanisicak O, Maillet M, Vagnozzi RJ, Karch J, Lin SC, Middleton RC, Marbán E, Molkentin JD. c-kit+ cells minimally contribute cardiomyocytes to the heart. Nature 2014;509:337–341.

25. Jin WN, Shi SX, Li Z, Li M, Wood K, Gonzales RJ, Liu Q. Depletion of microglia exacerbates postischemic inflammation and brain injury. J Cereb Blood Flow Metab 2017;37:2224–2236.

26. Gomes SA, Hare JM, Rangel EB. Kidney-derived c-kit(+) cells possess regenerative potential. Stem Cells Transl Med 2018;7:317–324.

27. Acar M, Kocherlakota KS, Murphy MM, Peyer JG, Oguro H, Inra CN, Jaiyeola C, Zhao Z, Luby-Phelps K, Morrison SJ. Deep imaging of bone marrow shows non-dividing stem cells are mainly perisinusoidal. Nature 2015;526:126–130.

28. Ni Z, Deng J, Potter CMF, Nowak WN, Gu W, Zhang Z, Chen T, Chen Q, Hu Y, Zhou B, Xu Q, Zhang L. Recipient c-kit lineage cells repopulate smooth muscle cells of transplant arteriosclerosis in mouse models. Circ Res 2019;125:223–241.

29. Inverso D, Shi J, Lee KH, Jakab M, Ben-Moshe S, Kulkarni SR, Schneider M, Wang G, Komeili M, Vélez PA, Riedel M, Spegg C, Ruppert T, Schaeffer-Reiss C, Helm D, Singh I, Boutros M, Chintharlapalli S, Heikenwalder M, Itzkovitz S, Augustin HG. A spatial vascular transcriptomic, proteomic, and phosphoproteomic atlas unveils an angiocrine Tie-Wnt signaling axis in the liver. Dev Cell 2021; 56:1677–1693.

30. Su T, Yang Y, Lai S, Jeong J, Jung Y, McConnell M, Utsumi T, Iwakiri Y. Single-cell transcriptomics reveals zone-specific alterations of liver sinusoidal endothelial cells in cirrhosis. Cell Mol Gastroenterol Hepatol 2021; 11:1139–1161.

31. Wang Y, Nakayama M, Pitulescu ME, Schmidt TS, Bochenek ML, Sakakibara A, Adams S, Davy A, Deutsch U, Lüthi U, Barberis A, Benjamin LE, Mäkinen T, Nobes CD, Adams RH. Ephrin-B2 controls VEGF-induced angiogenesis and lymphangiogenesis. Nature 2010;465:483–486.

32. Monvoisin A, Alva JA, Hofmann JJ, Zovein AC, Lane TF, Iruela-Arispe ML. VE-cadherin-CreERT2 transgenic mouse: a model for inducible recombination in the endothelium. Dev Dyn 2006;235:3413–3422.

33. Han H, Tanigaki K, Yamamoto N, Kuroda K, Yoshimoto M, Nakahata T, Ikuta K, Honjo T. Inducible gene knockout of transcription factor recombination signal binding protein-J reveals its essential role in T versus B lineage decision. Int Immunol 2002;14:637–645.

34. Wang L, Wang CM, Hou LH, Dou GR, Wang YC, Hu XB, He F, Feng F, Zhang HW, Liang YM, Dou KF, Han H. Disruption of the transcription factor recombination signal-binding protein-Jkappa (RBP-J) leads to veno-occlusive disease and interfered liver regeneration in mice. Hepatology 2009;49:268–277.

35. Tsujigiwa H, Hirata Y, Katase N, Buery RR, Tamamura R, Ito S, Takagi S, Iida S, Nagatsuka H. The role of bone marrow-derived cells during the bone healing process in the GFP mouse bone marrow transplantation model. Calcif Tissue Int 2013;92:296–306.

36. Yu X, Persillet M, Zhang L, Zhang Y, Xiuping S, Li X, Ran G, Breger LS, Dovero S, Porras G, Dehay B, Bezard E, Qin C. Evaluation of blood flow as a route for propagation in experimental synucleinopathy. Neurobiol Dis 2021;150: 105255.

37. Hall C, Rodriguez M, Garcia J, Posfai D, DuMez R, Wictor E, Quintero OA, Hill MS, Rivera AS, Hill AL. Secreted frizzled related protein is a target of PaxB and plays a role in aquiferous system development in the freshwater sponge, Ephydatia muelleri. PLoS One 2019;14:e0212005.

38. Regina C, Panatta E, Candi E, Melino G, Amelio I, Balistreri CR, Annicchiarico-Petruzzelli M, Di Daniele N, Ruvolo G. Vascular ageing and endothelial cell senescence: molecular mechanisms of physiology and diseases. Mech Ageing Dev 2016;159:14–21.

39. Ruan B, Duan JL, Xu H, Tao KS, Han H, Dou GR, Wang L. Capillarized liver sinusoidal endothelial cells undergo partial endothelial-mesenchymal transition to actively deposit sinusoidal ECM in liver fibrosis. Front Cell Dev Biol 2021;9:671081.

Correspondence
Address correspondence to: Lin Wang, PhD, Department of Hepatobiliary Surgery, Xi-Jing Hospital, Fourth Military Medical University, Xi'an 710032, China. e-mail: fierywang@163.com; fax: (86)-29-83246270. OR Guo-Rui Dou, PhD, Department of Ophthalmology, Xi-Jing Hospital, Fourth Military Medical University, Xi'an 710032, China. e-mail: douguorui@hotmail.com; fax: (86)-29-84771273. OR Hua Han, PhD, Department of Biochemistry and Molecular Biology, Fourth Military Medical University, Xi'an 710032, China; fax: (86)-29-84774516. e-mail: huahan@fmmu.edu.cn.

CRediT Authorship Contributions

Juanli Duan (Formal analysis: Equal; Investigation: Equal; Project administration: Equal)

Ziyi Zhou (Writing – original draft: Lead)

Bai Ruan (Formal analysis: Equal; Investigation: Equal; Project administration: Equal; Software: Lead)

Zhiqiang Fang (Formal analysis: Supporting; Methodology: Supporting)

Jian Ding (Methodology: Supporting)

Jingjing Liu (Methodology: Supporting; Resources: Supporting)

Ping Song (Methodology: Supporting)

Hao Xu (Methodology: Supporting)

Chen Xu (Methodology: Supporting)

Zhensheng Yue (Methodology: Supporting)

Hua Han (Supervision: Equal; Validation: Equal)

Guorui Dou (Supervision: Equal; Writing – original draft: Supporting; Writing – review & editing: Lead)

Lin Wang (Funding acquisition: Lead; Supervision: Lead; Validation: Lead; Writing – original draft: Equal; Writing – review & editing: Equal)